Publishing House
AKAPIT

COMPUTER METHODS IN MATERIALS SCIENCE

Informatyka w Technologii Materiałów

Vol. 13, 2013, No. 4

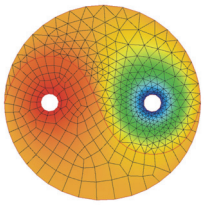

APPLICATION OF THE MULTISCALE MICROSTRUCTURE-BASED MODELLING TECHNIQUES FOR THE PREDICTION OF STRAIN INHOMOGENEITY IN THE NON-LINEAR DEFORMATION PROCESSES

KRZYSZTOF MUSZKA[1,*], PAULINA GRACA[1], MATEUSZ SITKO[1], ŁUKASZ MADEJ[1], LIN SUN[2]

[1] Faculty of Metals Engineering and Industrial Computer Science, AGH University of Science and Technology, 30 Mickiewicza Ave. 30-059 Kraków, Poland
[2] Department of Materials Science and Metallurgy, University of Cambridge, 27 Charles Babbage Road, Cambridge, CB3 0FS, United Kingdom
**Corresponding author: muszka@agh.edu.pl*

Abstract

The present paper discusses possibilities of combination of the Crystal Plasticity (CP) modelling with the 3D Digital Materials Representation (DMR) approach for the simulation of the non-linear deformation processes. Application of such modelling strategy as an extension of the existing multiscale model developed for prediction of the strain inhomogeneity during processes subjected to the complex strain paths, is presented and discussed. Two metal forming processes, characterised by non-linear loading conditions i.e. Accumulative Angular Drawing (AAD) process and the cyclic torsion deformation were chosen to verify the proposed modelling strategy. It is shown that thanks to a combination of the multiscale finite element model with the DMR and CP approach, detailed information on strain inhomogeneities and texture can be accurately obtained in both investigated processes.

Key words: 3D digital material representation, crystal plasticity, multiscale modelling, strain path changes

1. INTRODUCTION

For many decades, metal forming industry has evolved from relying on practical experience attained from trial and error tests in its early days to more and more complex numerical models for process optimisation and prediction of properties of manufactured products (Beynon & Sellars, 1992; Sellars, 1985; Sellars, 2011). Such models developed and improved by understanding the fundamental physics behind the microstructural changes and assisted by ever increasing computing power, are now standard tools for both: off-line optimisation and on-line control of thermo-mechanical processing.

For most industrial metal forming processes, the material is subjected to complex deformation histories with non-linear strain paths. In contrast, however, most of the current microstructural models have been developed based on the studies of microstructure evolution under simplified laboratory conditions, using monotonic deformation tests, i.e. linear strain paths, isothermal temperature or constant strain rate. Whilst these types of models are adequate in prediction of microstructure in the centre of the rolled plate, they are totally inadequate to predict the microstructure gradient through the whole thickness of rolled slab, especially near the surface of the rolled plate, where the strain path history is non-linear due to the shear deformation caused by the

ISSN 1641-8581

friction between the rolls and the stock material (Sellars, 2011).

Therefore, it is recognised that there is a need to develop new generation of models which are capable of predicting the local variations in microstructural evolution during metal forming when there are major changes in strain paths (Sellars, 2011).

In the present paper, further extension of the recently developed multiscale modelling strategy (Muszka, 2013; Muszka & Madej, 2013) is presented and used for the prediction of strain and texture inhomogeneity during metal forming processes involving complex strain path changes.

So far, in the previous version of the presented model, the orientation of the grains was taken into account only at the beginning of simulation via artificial diversification of the material model parameters and their assignment into each grain randomly, according to Gauss distribution function. However, such approach does not allow tracking of the grains' crystallographic orientation changes during deformation. Current stage of model development involves incorporation of the Crystal Plasticity (CP) model at the micro scale in order to allow tracking of texture changes during deformation. The CP method is generally considered as one of the most accurate approaches for the description of the material behaviour during deformation. This is because the method is based on the crystallographic aspects of deformation and takes into account such factors as slip in the slip planes, crystallographic orientation, and evolution of orientation.

2. EXPERIMENTAL INVESTIGATION

In order to provide data for the numerical modelling, two deformation processes, characterised by complex strain path changes, have been carried out i.e. Accumulative Angular Drawing (AAD) process and cyclic forward/reverse torsion test. These two particular processes have been chosen in order to verify the proposed model, as they are fully non-linear, and hence, they cannot be simulated using axisymmetric nor simple 2D models. Moreover, the textural changes in these two processes are complex and yet the ability of their prediction and optimisation is of a paramount importance.

2.1. Accumulative Angular Drawing (AAD) process

In the AAD process, high energy accumulation is utilised to deform the drawn wire to a higher strain, and thus, to refine its microstructure to much higher degree, compared to the typical linear wire-drawing process (Wielgus et al., 2010). Nb-microalloyed steel (0.07C/1.37Mn/0.27Si//0.07Nb/0.009N) supplied as a wire rod, with homogenous equiaxed ferrite microstructure and the mean grain size of 15μm, was used in this study. The 6.5mm diameter wire rods were drawn down to the diameter of 4 mm through the set of three dies (in two passes of drawing) with the total strain of 0.97 (Majta et al., 2012). Although the AAD design allows various combinations of die positioning to be used (figure 1), the present study was focused only on the stepped die positioning (figure 1c), in which the offset from the drawing line between the successive dies was equal to 15°.

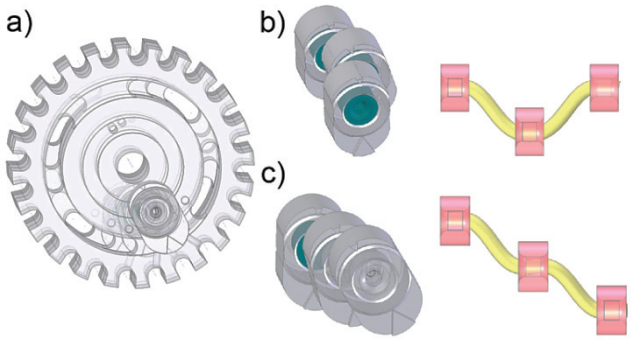

Fig. 1. *Schematic drawing of the AAD tool - front view - a) and examples of possible dies positionings: alternate - b) and stepped - c).*

The example results of the microstructure and texture study after AAD deformation are presented in figure 2. The wire drawing textures of bcc metals typically have <110> fibre texture component. In the AAD process, however, strain accumulation and inhomogeneity due to a complex deformation geometry (combination of drawing, bending, burnishing, shearing and torsion) lead to complex textures that are composed of drawing, shear and torsion texture components.

Moreover - as it can be seen in figure 2 - the texture after AAD process is inhomogeneous (with stronger intensities in near-surface areas), and thus, difficult to predict. After wire drawing and subsequent annealing, recovery and recrystallisation take place, leading to grain refinement and weakening of deformation texture. Due to the fact, that high deformation inhomogeneity and local strain concentrations are observed in the AAD process, the drawn wire displays more pronounced textures and strong through-diameter gradients in both textures and mi-

crostructures compared to the conventional drawing process (Majta et al., 2012).

The initial microstructure of the studied material is shown in figure 3a. Solid bar torsion specimens with gauge length of 20 mm and gauge diameter of

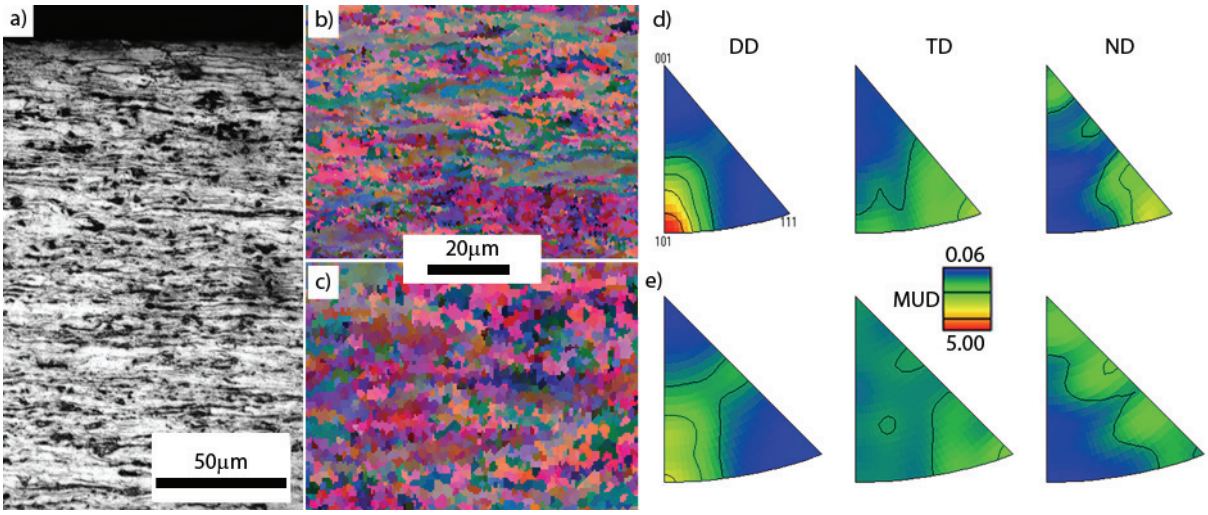

Fig. 2. *Optical micrograph showing deformed microstructure near the wire's surface (longitudinal cross-section - parallel to the drawing direction) -a); Euler maps and corresponding inverse pole figures taken near the surface -b), d) and in the middle -c), e) of the drawn wire.*

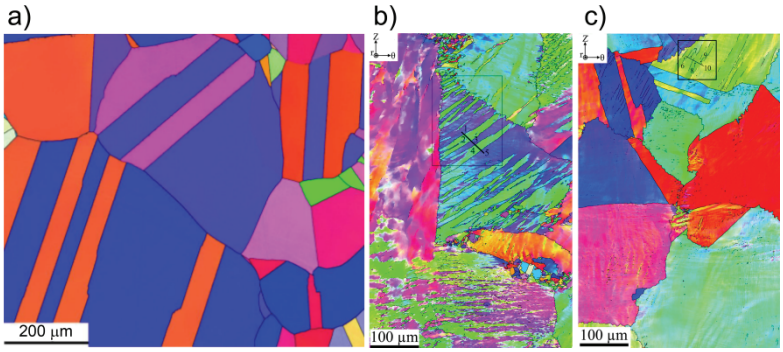

Fig. 3. *Electron Backscatter Diffraction (EBSD) map of the initial austenite microstructure –a), and the deformed microstructures after deformation using 2-pass -b) and 8-pass -c) torsion test respectively.*

The presented work confirmed that the strain path applied in the AAD process affects directly the microstructure and texture of the drawn wire. Because such a complex texture is difficult to predict in the AAD process, the use of numerical tools can be the only way to support its control and optimisation.

2.2. Forward/reverse torsion test

The effect of cyclic strain reversal on the austenite was studied in forward-reverse torsion tests using Fe-Ni model alloy system with a chemical composition of 0.092C-30.3Ni-1.67Mn-1.51Mo-0.19Si (the remainder being Fe - in wt. %). Fe-30wt.%Ni model alloys are widely used to study the behaviour of austenite as this phase is stable in these alloys down to the room temperature. Moreover, they have similar Stacking Fault Energy and high temperature flow behaviour to low carbon steels (Sun et al., 2011). 10 mm were deformed using servo-hydraulic torsion rig at 840ºC with strain rate of 1/s. Chosen deformation temperature is well below recrystallization stop temperature. Two deformation schedules were applied, both with the same equivalent total strain of 2. In the first case, 4 cycles of forward/reverse with strain of 0.25 per pass (8-passes in total) were applied. In the second case, 2-passes of deformation with the strain of 1 per pass and only one reversal were applied.

Deformed microstructures observed using EBSD analysis are presented in figure 3b and c (Sun et al., 2011). It can be seen that upon strain reversal, the original shape of austenite grains has been restored in both cases. In the case of 2-pass deformation, however, the initial austenite microstructure has been subdivided into well-developed lamellar structures separated by high angle grain boundaries (figures 3b and 4a). More detailed EBSD analysis

showed that in the case of 2-pass test, local orientations measured by the <111> pole figures (shown in figure 4b) indicate the orientations of the lamellar subgrains alternating between two texture components. Furthermore, it is quite clear that one set of the subgrain orientations is aligned with an ideal torsion (shear) texture component (Barnett & Montheillet, 2002; Toth et al., 1989), whilst the other set appears to be non standard. It is also noticed that the majority of rotation axes between 2 and 90 degrees are closely aligned with the *r* direction in the deformation geometry (figure 4c) which is the invariant direction during torsion deformation. The above observations suggest that the origin of the new HAGBs during hot deformation of austenite is similar to the texture mechanism which was reported in aluminium alloys by (Hughes & Hansen, 1997): under straining, crystallites within individual grains such as cell blocks of different active slip systems eventually rotate to different preferred end orientations or to the same stable orientation but at different speeds (Barnett & Montheillet, 2002).

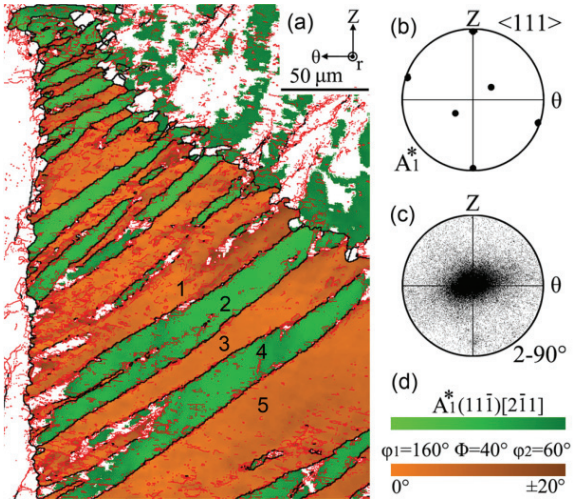

Fig. 4. *Detailed EBSD analysis of the 2-pass specimen: (a) texture component map showing ideal shear texture component A_1* as green and non-standard component with Euler angles of φ1=160°, Φ=40° and φ2=60° shown as brown both with maximum 20° deviation. Red lines represent LABs>2°. (b) <111> pole figure of A1* component and (c) rotation axes with respect to macroscopic coordinates. (d) legend for the colouring method in the texture component map.*

For the 8-pass cyclical deformation to the same strain of 2.0 (figures 3c and 5a), there are well developed substructures within the original austenite grains but the HAGBs (black lines) generated by grain subdivision are quite limited. The misorientation angle/axis line scan revealed that these HAGBs have similar features but relatively lower disorientation angles (20°~30°) compared to those from the 2-pass test. In this case, the <111> pole figures of subgrain 6 and 8 (figure 5a) are similar to the ideal A2* (11-1)[112] (Z-θ) shear texture component which is shown by the <111> pole figure in figure 5b.

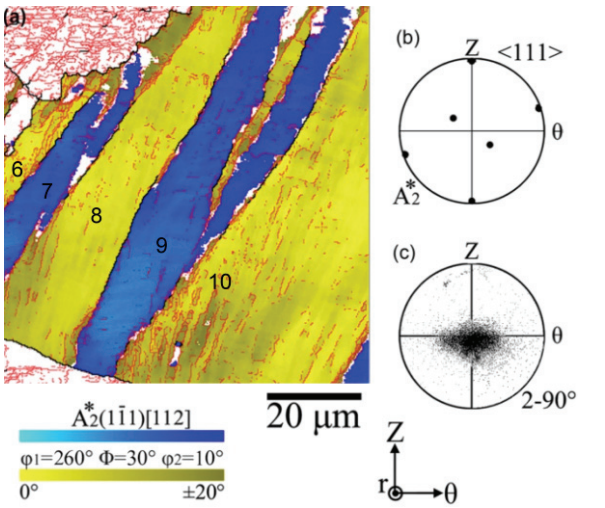

Fig. 5. *Detailed EBSD analysis of 8-pass specimen: (a) texture component map showing ideal shear texture component A2* as blue and non-standard component with Euler angles of φ1=260°, Φ=30° and φ2=10° as yellow both with maximum 20° deviation. Red lines represent LABs>2°. (b) <111> pole figure of A2* component and (c) rotation axes with respect to macroscopic coordinates.*

More interestingly, figure 5a shows that some of the boundaries separating the two texture components were mixtures of LABs (red) and HABs (black). This observation suggests a possible transition from microstructure/dislocation-accumulation mechanism to texture/subgrain-rotation mechanism for generating HAGBs.

The present study confirms that strain path effect represents one of the most important processing parameters characterising hot metal forming processes. Based on the above observations, it can be summarised that the amount of new HAGBs formed by the texture mechanism is sensitive to the strain path because there is a threshold strain level for monotonic deformation to produce HAGBs when preferred stable orientations are well developed. Below this threshold strain, no or only very limited amount of HAGBs can be developed by the texture mechanism. This affects the number of possible nucleation sites for the subsequent phase transformation and its products what in turn has a direct impact on the properties of the final products. Therefore, proper computer model taking into account the above-mentioned phenomena can put some new insight into understanding and optimisation of the processes carried out under complex loading conditions.

3. NUMERICAL MODELLING

The main aim of the present work is a further development of the modelling framework that has been proposed in (Madej et al., 2011b) and already used in (Muszka, 2013; Muszka & Madej, 2013). The original multiscale model was designed to predict the strain inhomogeneity during deformation processes characterised by a complex strain path changes. Its strain path sensitivity was achieved thanks to the utilisation of the combined isotropic-kinematic material model, instead of a pure isotropic model (Madej et al., 2011a). As it was already shown, the original model, thanks to the incorporation of the 3D Digital Materials Representation (Madej et al., 2011b) and multiscale approach, resulted in much higher accuracy in terms of strain inhomogeneity predictions compared to standard macro scale models. On top of that, application of a full 3D approach allowed for complex loading cases to be effectively modelled.

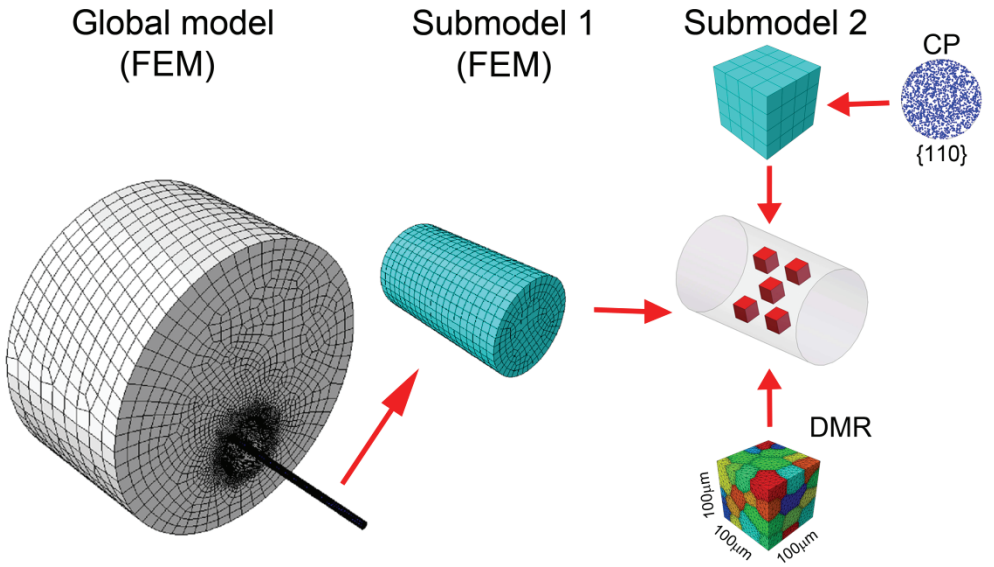

Fig. 6. *Concept of the multiscale model of the AAD process.*

Current stage of model development involves incorporation of the CP-FEM model at the micro scale in order to allow tracking of texture changes during deformation. So far, the orientation of the grains was taken into account only at the beginning of the process, via artificial diversification of the material model parameters and their assignment into each grain randomly, according to Gauss distribution function. Such approach, however, does not allow modelling of the texture development during deformation. The CP models make use of the basic principles of mechanics to achieve transition from the macro to micro scale (e.g., the stress equilibrium and the geometrical compatibility at the individual grain boundaries). In this approach, the plastic deformation occurs due to crystallographic dislocation slip, while other factors, such as diffusion, twinning, and grain boundary sliding, are not taken into account (Cao et al., 2010).

In the present work, two types of CP models have been chosen and tested in terms of their applicability for modelling of the processes characterised by strain path changes and are presented in the following chapters.

3.1. CP multiscale model of the AAD process

Multiscale model of the AAD process due to its complexity requires two steps of submodelling as presented in figure 6. First, global model with 42000 eight-node hexagonal reduced integration elements with hourglass control (C3D8R) was realized using Abaqus Explicit. Drawing of 300 mm long wire with the initial diameter of 6.5mm was modelled. Tools were meshed with quad-dominated discrete rigid elements (R3D). Furthermore, the analysis was repeated on the smaller cylindrical area (10 mm long) subdivided from the global model using Abaqus Standard and much finer mesh was used. The second submodel was generated using the 3D DMR approach and calculations were performed again, using Abaqus Standard. Set of 5 unit cells (100 μm ×100 μm × 100 μm) containing 37 grains each was created to capture the effect of the process on inhomogeneity of both strain and microstructure.

Finally, at the micro level – submodel 2 (see figure 6) – besides of the unit cells with DMRs, additional submodels were created where CP model (Groh et al., 2009; Cyberinfrastructure for ICME, 2013) was combined with the Finite Element Model (FEM) and used to predict the texture evolution at the various positions of the cross-section of the drawn wire. In this model, description for the kinet-

ics of the α-slip system is based on the well-known power law function given by:

$$\dot{\gamma}^{\alpha} = \dot{\gamma}_0 \left[\frac{\tau^{\alpha}}{\kappa^{\alpha}} \right]^{1/m} \tag{1}$$

where γ^{α} is the applied shear stress on the α-slip system, $\dot{\gamma}^{\alpha}$ is the shear strain rate, $\dot{\gamma}_0$ is a reference shear strain rate, and κ^{α} is the slip system strength or hardness. The strain rate sensitivity exponent, m, and the reference shear rate are defined as:

$$m = \frac{kT}{\alpha \mu b^2 d} \quad \text{and} \quad \dot{\gamma}_0 = \rho_m b^2 \upsilon_D \exp\left(\frac{-\Delta G_0}{kT} \right) \tag{2}$$

where T is temperature, k is Boltzmann constant, μ is the shear modulus, α is the average strength of the dislocation forest, b is the length of Burgers vector, d is distance to bypass the obstacle, v_D is the Debye frequency, ρ_m is the density of mobile dislocations and the ΔG_0 is the energy stored in the material when an obstacle is bypassed by moving dislocation.

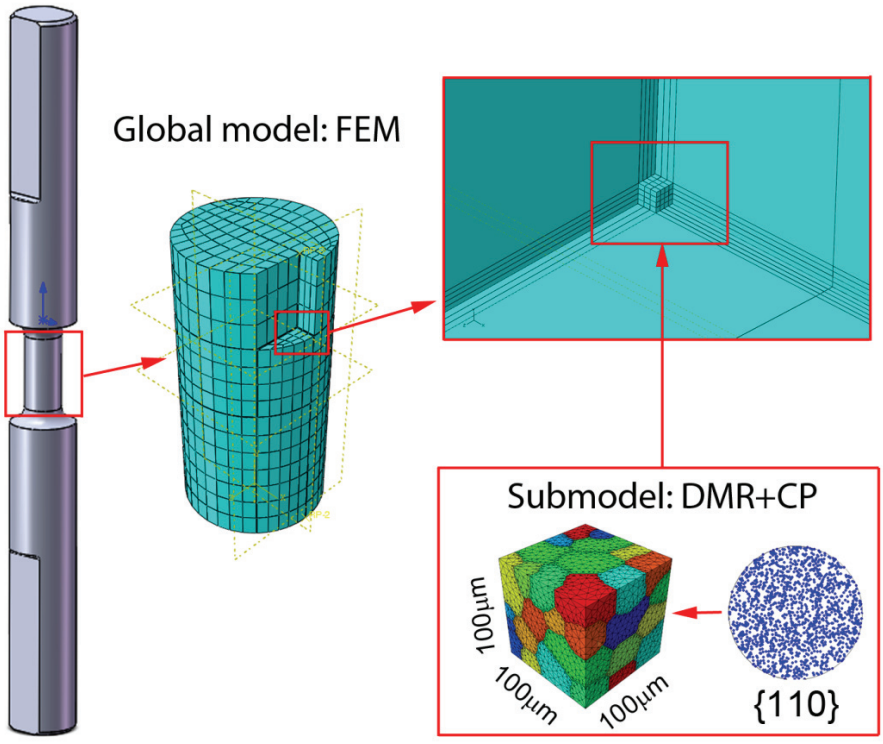

Fig. 7. *Multiscale model of the cyclic torsion test.*

In the present model the slip system hardening rule is described by the following scalar form:

$$\dot{\kappa}^{\alpha} = h_0 \left(\frac{\kappa_s - \kappa}{\kappa_s - \kappa_0} \right) \sum_{\alpha} \left| \gamma^{\alpha} \right| \tag{3}$$

where h_0 is the initial hardening rate, κ_0 is the initial strength, and κ_s is the saturation strength. Presented model was implemented into Abaqus Standard code using UMAT subroutine. At the current stage, the parameters of the CP model were taken from (Tikhovskiy et al., 2008). As the input, 500 random crystallographic orientations were assigned into each of the unit cells, that were put into different positions at the wire's cross section. As the output, besides of the strain and stress distributions, evolution of texture was calculated and saved into a text file in the form of Euler angles (in Kocks' convention). In order to present the results of texture calculation, the pole figures were plotted subsequently using Mtex Matlab Toolbox (Hielscher & Schaeben, 2008).

3.2. CP multiscale model of the cyclic torsion test

The multiscale model of the torsion test was designed according to figure 7. Similarly to the previous case, submodelling technique was used here to bridge the different length scales. Global model of the whole strain gauge was done in Abaqus Standard. Next, the submodel was generated using the DMR approach and calculations were performed again. A unit cell (100 µm × 100 µm × 100 µm) with 37 grains was created to capture the effect of the process on inhomogeneity of both strain and microstructure.

In this case - on the contrary to the AAD process - the CP-FEM model is incorporated directly into the DMR unit cell. It is expected that this way, the accuracy of the predicted texture will be further increased. The CP-FEM model used here is also different to the previous one. In this classic CP model, the total deformation gradient consists of two terms: stretching and rotation $\mathbf{F}^{*}$, and plastic shear $\mathbf{F}^{p}$:

$$\mathbf{F} = \mathbf{F}^{*}\mathbf{F}^{p} \tag{4}$$

The velocity gradient in the current state is decomposed into the symmetric rate of stretching $\mathbf{D}$

and asymmetric spin tensor **W**. These two tensors consist of lattice parts and plastic parts:

$$\begin{aligned} \mathbf{D} &= \mathbf{D}^{*} + \mathbf{D}^{\mathrm{p}} \\ \mathbf{W} &= \mathbf{W}^{*} + \mathbf{W}^{\mathrm{p}} \end{aligned} \tag{5}$$

where: **D***, **W*** – lattice parts of the rate of stretching and spin tensor, $\mathbf{D}^{\mathrm{p}}$, $\mathbf{W}^{\mathrm{p}}$ – plastic part of the rate of stretching and spin tensor.

The decomposition must satisfy the following conditions:

$$\begin{aligned} \mathbf{D}^{*} + \mathbf{W}^{*} &= \dot{\mathbf{F}}^{*}\mathbf{F}^{*-1} \\ \mathbf{D}^{\mathrm{p}} + \mathbf{W}^{\mathrm{p}} &= \sum_{\alpha} \dot{\gamma}^{(\alpha)} \mathbf{s}^{*(\alpha)} \mathbf{m}^{*(\alpha)} \end{aligned} \tag{6}$$

where: $\dot{\gamma}^{(\alpha)}$ – slipping rate on slip system α, $\mathbf{s}^{*(\alpha)}$, $\mathbf{m}^{*(\alpha)}$ – slip direction and normal to slip plane in local coordinates for slip system α. The slip direction and normal to slip plane are related to both the local and global coordinate systems.

$$\begin{aligned} \mathbf{s}^{*(\alpha)} &= \mathbf{F}^{*}\mathbf{s}^{(\alpha)} \\ \mathbf{m}^{*(\alpha)} &= \mathbf{m}^{(\alpha)}\mathbf{F}^{*-1} \end{aligned} \tag{7}$$

where: $\mathbf{s}^{(\alpha)}$, $\mathbf{m}^{(\alpha)}$ – slip direction and normal to slip plane in global coordinates for slip system α. The crystalline slip in the model is controlled by the Schmid law. The Schmid stress depends on the current stress state **σ** and the current lattice orientation described by:

$$\tau^{(\alpha)} = \mathbf{m}^{*(\alpha)} \boldsymbol{\sigma} \mathbf{s}^{*(\alpha)} \tag{8}$$

The amount of shear on a slip system $\dot{\gamma}^{(\alpha)}$ is calculated based on the Schmid law. For rate-dependent crystalline, it is determined by:

$$\dot{\gamma}^{(\alpha)} = \dot{a}^{(\alpha)} \frac{\tau^{(\alpha)}}{g^{(\alpha)}} \left| \frac{\tau^{(\alpha)}}{g^{(\alpha)}} \right|^{n-1} \tag{9}$$

where: $\dot{a}^{(\alpha)}$ – reference strain rate of slip system α, n – stress sensitivity parameter, $g^{(\alpha)}$ – current strength for slip system α:

$$\dot{g}^{(\alpha)} = \sum_{\beta} h_{\alpha\beta} \dot{\gamma}^{(\beta)} \tag{10}$$

$$h_{\alpha\beta} = \begin{cases} h(\gamma) = h_0 sech^2 \left| \dfrac{h_0 \gamma}{\tau_s - \tau_0} \right| & \alpha = \beta \\ q h(\gamma) & \alpha \neq \beta \end{cases} \tag{11}$$

where: $h_{\alpha\beta}$ – matrix of hardening modules that describes self and latent hardening of slip systems, h_0 – initial hardening modulus, τ_s – shear stress where large plastic flow initiates, τ_0 – critical resolved shear stress yield stress, q – constant, γ – cumulative slip strain.

In the present work, the CP-FEM was implemented at the micro level of the models of cyclic torsion test, where the unit cells are simulated using DMR technique. The CP-FEM strategy is incorporated here using the UMAT subroutine and thus, it replaces the combined hardening model that was originally used. The initial orientations of the grains are assumed random. The texture evolution is calculated during the first cycle of strain reversal for two strain paths - i.e. forward/forward and forward/reverse torsion.

4. RESULTS OF NUMERICAL MODELLING

The main aim of the present work is to assess the possibilities of capturing textural changes in the processes characterised by complex loading conditions. In the first part of the work, the texture evolution and inhomogeneity was modelled in the AAD process at the micro scale using unit cells attached at various positions of the cross-section of the drawn wire. In the second part of the work, CP-FEM model was combined directly with the DMR and used to study the texture changes during torsion test.

4.1. CP-FEM model of the AAD process

Example results of the simulation of the AAD process using presented multiscale model are shown in figure 8. It can be noticed that the inhomogeneity of stress that is characteristic for this deformation process was properly captured by the applied model. Application of the submodelling technique combined with DMR approach significantly improved the accuracy of the results compared to global model only (figure 8c). Also, strain inhomogeneity on the cross section after subsequent deformation stages corresponds to the earlier observations in the microstructure analysis.

{110} pole figures simulated after AAD process are presented in figure 8a together with the initial, random texture. Because of the complexity of the process it is not possible to track the textural changes during deformation using experimental tools, and thus, the direct quantitative comparison is not possible. Nevertheless, the qualitative analysis of the

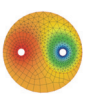

results shows that significant texture inhomogeneity was generated in the cross-section of the wires, that was also observed from the EBSD results (see: figure 2). Comparison of calculated (CP-FEM) and measured textures (EBSD) in the surface area of the drawn wire, that is shown in figure 9b, also supports this statement. It can be noticed that the pole figures are correctly represented what shows the potential of the proposed strategy. Based on these preliminary results it can be summarised that by the combination of the CP-FEM and multiscale modelling approach it may be possible to predict and optimise texture and microstructure inhomogeneities in the processes characterised by complex non-linear loading conditions. However, more detailed quantitative analysis requires further work and more experimental data.

strain, microstructure and texture inhomogeneity with a reasonably good accuracy.

4.2. CP-FEM model of the torsion test

In the simulation of the cyclic torsion test - on the contrary to the AAD process - each grain in the unit cell of DMR was modelled using CP model (presented in the paragraph 3.2) assigned directly. It allowed to track the textural changes in the grains as well as to predict the equivalent strain and stress distributions. Comparison of the shear strain distribution calculated in the unit cells after two various strain path: forward/forward and forward/reverse torsion deformation as well as in the global model is presented in figure 10. It can be seen that application

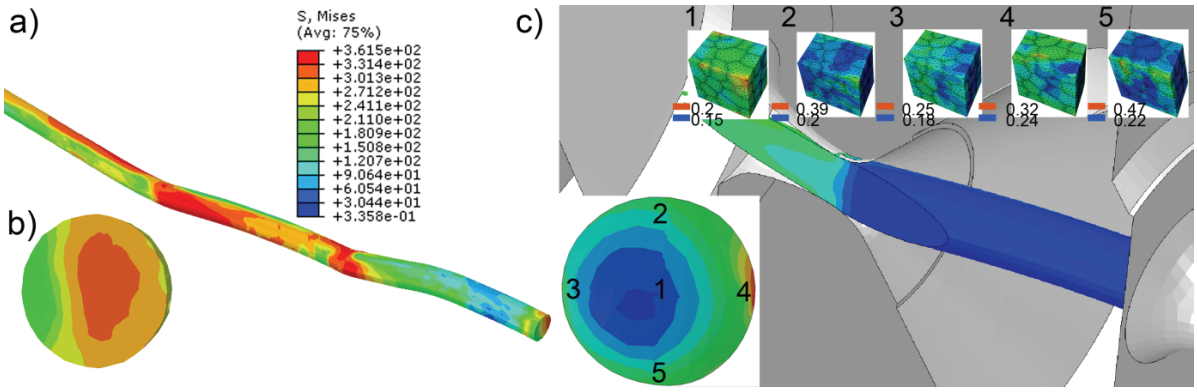

Fig 8. Example results from AAD process simulation: von Mises stress distribution in global model - a), b) and equivalent strain distribution in global and local models - c).

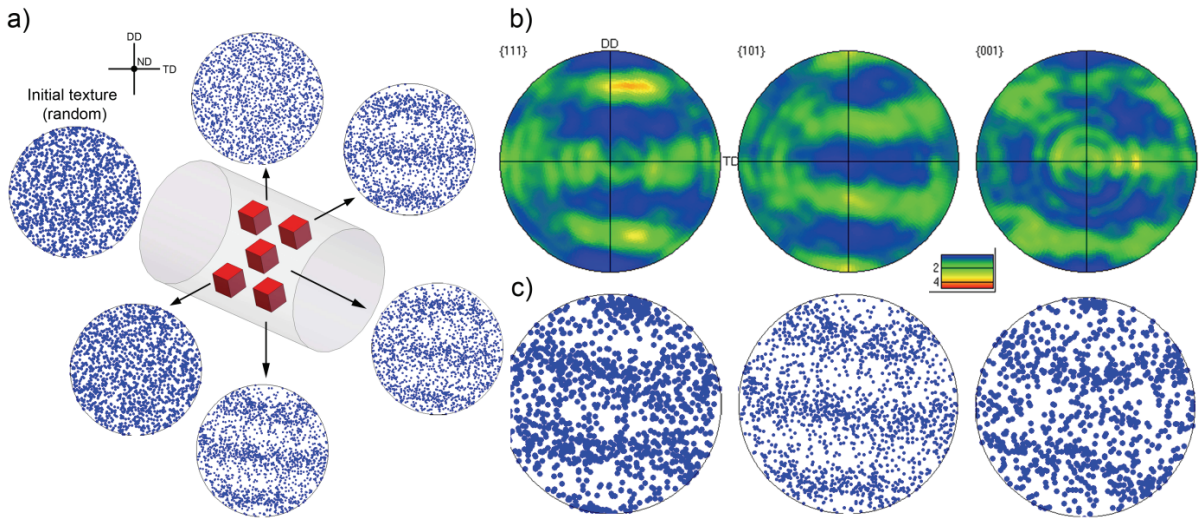

Fig. 9. Results of CP-FEM calculations: texture inhomogeneity in the cross-section of the drawn wire - a), comparison of the measured and calculated pole figures - b).

Based on the presented procedures of the computer modelling, it can be stated that the applied modelling approach was able to catch most of the important phenomena accompanying the AAD process. Presented strategy allows for simulation of

of the submodelling technique with combined DMR significantly improved the accuracy of the results compared to the macro model.

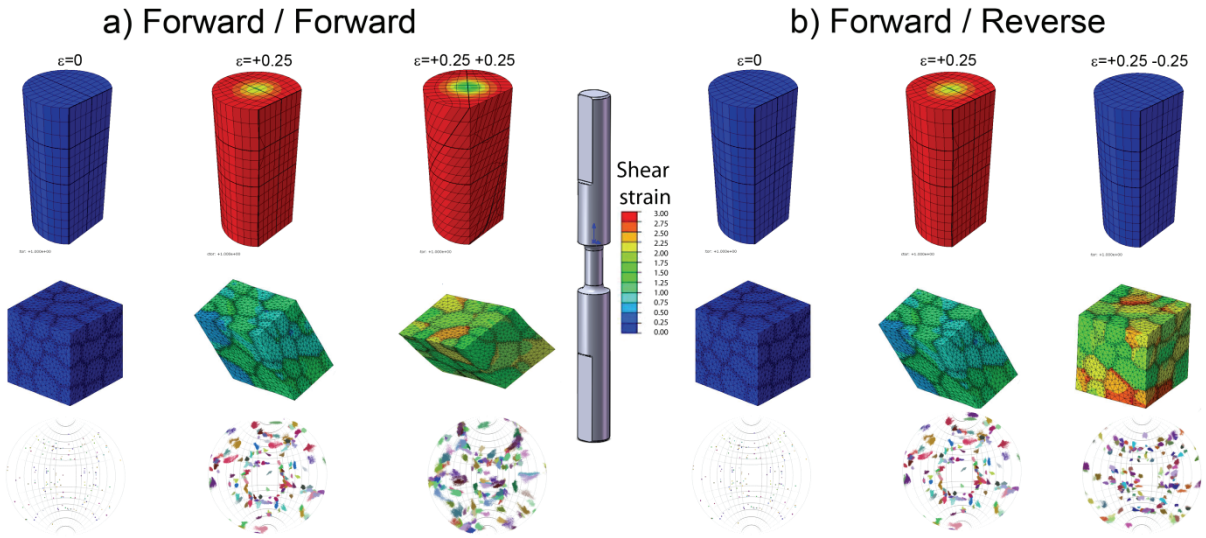

Fig. 10. *Example of simulation results: shear strain distribution in global models and unit cells along with the corresponding texture calculated after deformation with Forward/Forward - a) and Forward/Reverse - b) deformation routes.*

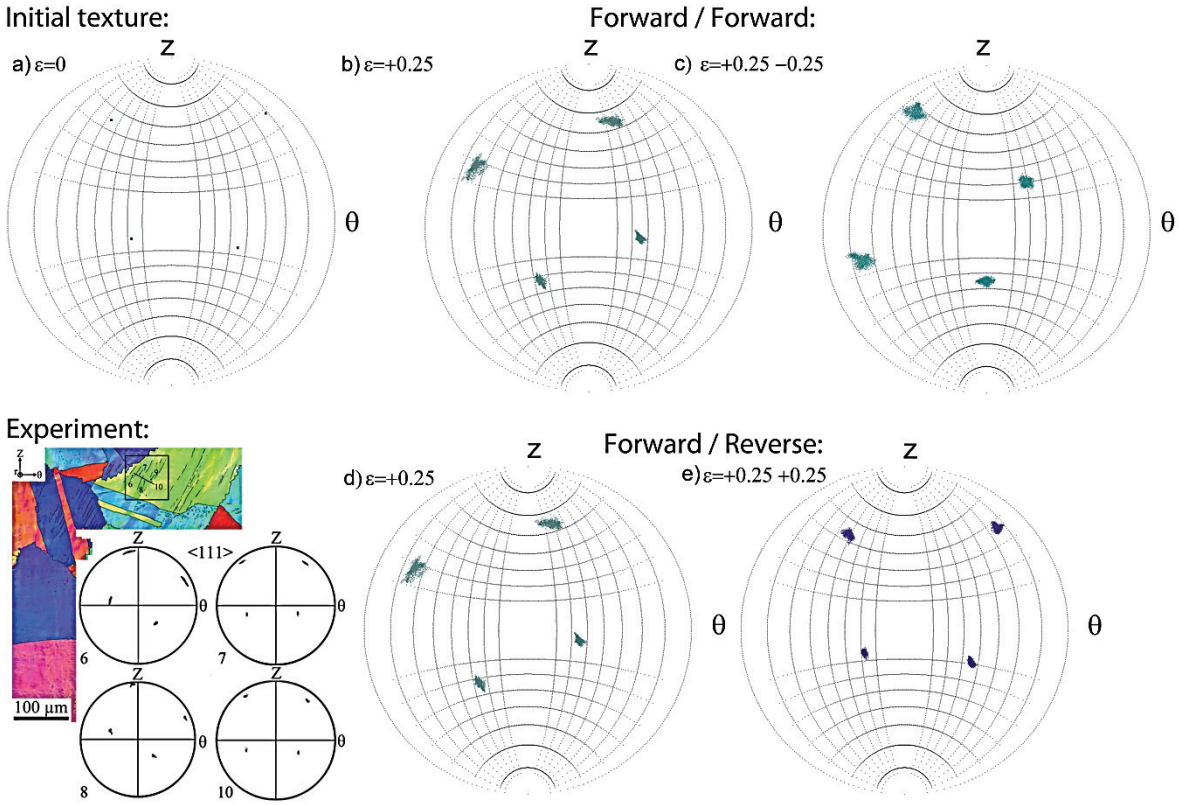

Fig. 11. *Comparison of the simulated pole figures extracted from a single grain after deformation with Forward/Forward - a), - b, - c) and Forward/Reverse - a), - d, - f) deformation routes and experimental data.*

Moreover, 3D DMR properly captured not only stress state but also grain shape changes – as an effect of strain reversal. It can be seen that the first pass of forward/reverse cyclic deformation caused grains rotation. Their original positions were then restored after strain reversal and application of the second pass of deformation with the same strain level applied in the opposite torsion direction.

The further advantage of this approach is the capability to track the textural changes at the grains level. The pole figures for the single grains extracted from unit cell deformed with various deformation routes are also summarised in figure 11 and compared with the data from experiment. It can be observed that strain reversal caused the grain to return not only to its original shape but also to its original crystallographic orientation (figure 11a-c) whereas

during deformation with no strain reversal, further grain rotation was observed. This is consistent with the data observed during experiments (figure 11) what proves the accuracy of the presented methodology and shows its potential in simulations of the processes with cyclic strain path changes.

5. CONCLUSIONS

The main aim of the present work was a further development of the modelling framework designed to predict the strain inhomogeneity during deformation processes characterised by a complex strain path changes. An attempt to extend this model towards its capability to predict textural changes in the above-mentioned processes was made. In the first part of the work, the texture evolution and inhomogeneity was modelled in the AAD process at the micro scale in the unit cells attached at various positions of the cross-section of the drawn wire. In the second part of the work, CP-FEM model was combined directly with the DMR and used to study the texture changes during torsion test.

Based on the presented modelling results it can be concluded that the applied modelling strategy was able to catch most of the important phenomena accompanying processes with complex deformation modes with reasonably good accuracy.

ACKNOWLEDGEMENTS

Financial support from the National Science Centre Poland (grant no. DEC-2012/05/D/ST8/02367) is gratefully acknowledged. FEM calculations were realised at ACK AGH Cyfronet Computing Centre under grant no: MNiSW/IBM_BC_HS21/AGH/075/2010.

Authors are also grateful to Prof. J. Majta from AGH University of Science and Technology (Krakow, Poland) for granting access to the results from the AAD process and to Dr Eric Palmiere from The University of Sheffield for granting access to the Arbitrary Strain Path Machine.

REFERENCES

Barnett, M. R., Montheillet, F., 2002, The Generation of New High-Angle Boundaries in Aluminium During Hot Torsion, *Acta Materialia*, 50, 2285-2296.

Beynon, J. H., Sellars C. M., 1992, Modeling Microstructure and Its Effects During Multipass Hot-Rolling, *ISIJ International*, 32, 359-367.

Cao, J., Zhuang, W., Wang, S., Lin, J., 2010, Development of a VGRAIN system for CPFE analysis in micro-forming applications, *International Journal of Advanced Manufacturing Technology*, 47, 981-991.

Cyberinfrastructure for ICME, 2013, Code: ABAQUS CPFEM, available online at: https://icme.hpc.msstate.edu/mediawiki/index.php/Code:_ABAQUS_CPFEM, last access: 22.01.2014

Groh, S., Marin, E.B., Horstemeyer, M.F., Zbib, H.M., 2009, Multiscale modeling of the plasticity in an aluminum single crystal, *International Journal of Plasticity*, 25, 1456-1473.

Hielscher, R., Schaeben, H., 2008, A novel pole figure inversion method: specification of the MTEX algorithm, *Journal of Applied Crystallography*, 41, 1024-1037.

Hughes, D.A., Hansen, N., 1997, High Angle Boundaries Formed by Grain Subdivision Mechanisms, *Acta Materialia*, 45, 3871-3886.

Madej, L., Muszka, K., Perzynski, K., Majta, J., Pietrzyk, M., 2011a, Computer aided development of the levelling technology for flat products. *CIRP Annals - Manufacturing Technology*, 60, 291-294.

Madej, L., Rauch, L., Perzynski, K., Cybulka, P., 2011b, Digital Material Representation as an efficient tool for strain inhomogeneities analysis at the micro scale level, *Archives of Civil and Mechanical Engineering*, 11, 661-679.

Muszka, K., 2013, Modelling of deformation inhomogeneity in the angular accumulative drawing process — multiscale approach. *Materials Science and Engineering A*, 559, 635-642.

Muszka, K., Madej, L., 2013, Application of the three dimensional digital material representation approach to model microstructure inhomogeneity during processes involving strain path changes, *Computer Methods in Materials Science*, 13, 258-263.

Sellars, C. M., 1985, Computer Modelling of Hot-Working Processes, *Materials Science and Technology*, 1, 325-332.

Sellars, C. M., 2011, From Trial and Error to Computer Modelling of Thermomechanical Processing, *Ironmaking & Steelmaking*, 38, 250-257.

Sun, L., Muszka, K., Wynne, B.P., Palmiere, E.J., 2011, The effect of strain path reversal on high-angle boundary formation by grain subdivision in a model austenitic steel, *Scripta Materialia*, 64, 280-283.

Tikhovskiy, I., Raabe, D., Roters, F., 2008, Simulation of earing of a 17% Cr stainless steel considering texture gradients, *Materials Science and Engineering A*, 488, 482-49.

Toth, L. S., Neale, K. W., Jonas, J.J., 1989, Stress Response and Persistence Characteristics of the Ideal Orientations of Shear Textures, *Acta Metallurgica*, 37, 2197-2210.

Wielgus, M., Majta, J., Łuksza, J., Packo, P., 2010, Effect of strain path on mechanical properties of wire drawing products, *Steel Research International*, 81, 490-493.

ZASTOSOWANIE TECHNIK MODELOWANIA WIELOSKALOWEGO WYKORZYSTUJĄCYCH PODEJŚCIE MIKROSTRUKTURALNE DO PRZEWIDYWANIA NIEJEDNORODNOŚCI ODKSZTAŁCENIA W PROCESACH CHARAKTERYZUJĄCYCH SIĘ NIELINIOWĄ ŚCIEŻKĄ ODKSZTAŁCANIA

Streszczenie

W artykule omówiono możliwości zastosowania połączenia modeli Plastyczności Kryształu z trójwymiarowym modelem Cyfrowej Reprezentacji Materiału do symulacji procesów charakteryzujących się nieliniową ścieżką odkształcania. Podejście to zastosowano do rozbudowy istniejącego wieloskalowego modelu opartego na metodzie elementów skończonych, którego możliwości zweryfikowano i przedyskutowano na przykładzie dwóch wybranych procesów przeróbki plastycznej, zachodzących w złożonym stanie odkształcenia tj. procesu Kątowego Wielostopniowego Ciągnienia (KWC) oraz próby cyklicznego skręcania. Wykazano, że dzięki zastosowaniu podejścia wieloskalowego oraz jego połączeniu z Cyfrową Reprezentacją Materiału oraz Plastycznością Kryształu możliwe jest uzyskanie szczegółowych i dokładnych informacji o niejednorodności odkształcenia i tekstury w symulacjach wybranych procesów.

Received: December 22, 2013
Received in a revised form: January 3, 2014
Accepted: January 8, 2014